Electronic Structure and Vibrational Modes of Cobalt Oxide Clusters CoO_n ($n = 1-4$) and Their Monoanions

Ellie L. Uzunova,[†] Georgi St. Nikolov,*[,†] and Hans Mikosch[‡]

Institute of General and Inorganic Chemistry, Bulgarian Academy of Sciences, Sofia 1113, Bulgaria, and Institute of Solid State Chemistry and Technical Electrochemistry, Vienna University of Technology, Vienna 1060, Austria

Received: November 29, 2001; In Final Form: February 5, 2002

The stationary points on the potential energy surfaces (PES) of cobalt oxide clusters were studied by the density functional theory, with the B1LYP exchange-correlation functional. A number of local minima were detected on the doublet, quartet, and sextet PES of CoO_n ($n = 1-4$) and the singlet, triplet, and quintet PES of the corresponding anions. The normal vibrations of all optimized structures were calculated and interpreted in terms of group theory. The global minima and the low-lying local minima have been also examined by the coupled-cluster method with single and double substitutions and perturbational estimate of triple excitations, CCSD(T). The ground state of CoO is a quartet ($^4\Delta$), in agreement with previous assignments, while the ground state of CoO^- is a quintet ($^5\Delta$). The oxides CoO_2 are more stable than the peroxides $Co(O_2)$. The neutral oxide CoO_2 in its ground state $^6A_1$ is quasilinear; the monoanion in its $^5\Delta_g$ ground state is linear. Oxoperoxides $OCo(O_2)$ are more stable than oxides CoO_3 and superoxides OCoOO. Diperoxides are the stable structures for the uncharged CoO_4. In general, the monoanions are more stable than the neutral clusters; however, electron attachment to peroxide destabilizes the O−O bond. The ground states of CoO_n ($n = 2-4$) and the ground states of their anions $[CoO_n]^-$ are high-spin states—sextets for the neutral species and quintets for the anions. The thermodynamic stability of different structures was examined for possible fragmentation paths. The CoO_n clusters and their monoanions dissociate preferably with the release of a dioxygen molecule.

Introduction

Transition metals interact with oxygen in many catalytic, electrochemical, and biological processes.[1] In recent years, a number of theoretical studies have been devoted to metal oxide clusters.[2−10] The results, reported for main group element oxides are definitive,[2−4] and a number of problems due to the interactions between the large number of electrons in oxides of the second and third transition row have now been resolved.[5] The first row (3d) elements and their compounds are still a serious challenge for theoretical treatment.[11−14] Near-degeneracy effects, s−d energy separation, and the specific orientation of the d-orbitals are only a part of the problem. Among the compounds of the 3d-elements, cobalt is the least studied element from a theoretical point of view. Difficulties arise from the abundance of various minima on the potential energy surface, closely spaced valence orbital levels, and small HOMO−LUMO energy gaps.[12,13] Most of the experimental data on cobalt oxide species refer to CoO.[15,16] Higher cobalt oxidation states in CoO_n ($n = 1-4$) have been obtained by the reaction of laser-ablated cobalt atoms with oxygen; their IR spectra have been measured in a Ar matrix.[17] The IR spectra of ^{18}O-substituted cobalt oxide species[17] and ESR data[18] suggest the presence of linear OCoO in a doublet ground state. Cyclic $Co(O_2)-\eta^2$-complexes and side-on η^1-complexes were also detected.[17] They represent a certain interest for homogeneous catalytic reactions and oxygen transportation in biological systems.

Cobalt oxide molecules CoO_n ($n = 1-4$) and their anions $[CoO_n]^-$ are examined here by the DFT formalism in order to detect the global and local minima on potential energy surfaces of the allowed spin multiplicities. The energetics and the harmonic vibrational frequencies are also examined as well as the thermodynamic stability, local magnetic and electric properties, and electron affinity of the neutral species.

Methods

Geometry optimization and harmonic frequency calculations were performed by the B1LYP method, which includes local and nonlocal terms as implemented in the Gaussian 98 package.[19−22] The Becke one-parameter functional was derived from the B3LYP functional,[23] the three parameters being substituted by one. The standard 6-311+G* basis set was employed, namely, Co[10s7p4d1f] and O[5s4p1d]. Potential energy surface scans were performed for the three-atomic configurations CoO_2 at steps of $R_{Co-O} = 0.05$ Å and $\angle OCoO = 5°$. Harmonic vibrations were analyzed for all the optimized geometries in order to determine the nature of the resulting stationary points. The minima on the potential energy surfaces were qualified by the absence of negative eigenvalues in the diagonalized Hessian matrix, giving imaginary normal vibrational modes. Coupled-cluster singles and doubles single-point calculations, including noniterative triples, CCSD(T)[24−29] have been performed with the B1LYP-optimized geometries for the lowest energy states.

Electron spin density and charge distribution on the atoms have been calculated following the Mulliken population scheme.[30] Electron spin density on cobalt and oxygen in the diatomic molecules calculated as the difference between α and β natural orbital populations[31−33] produced very similar results.

[†] Bulgarian Academy of Sciences.
[‡] Vienna University of Technology.

10.1021/jp0143692 CCC: $22.00
Published on Web 03/27/2002

TABLE 1: Bond Lengths and Vibrational Frequencies for Oxygen Species

	O_2	O_2^-	O_2^{2-}	O_3	O_3^{2-}
state	$^3\Sigma_g^-$	$^2\Pi_g$	$^1\Sigma_g^+$	$^1A_1$	$^1A_1$
R_{O-O}, Å	1.203	1.343	1.565	1.252	1.482
R_{O-O}, Å, exp.	1.208[a]	1.35[a]	1.49[a]	1.278[c]	
$\angle O_{(2)}O_{(1)}O_{(2)}$, deg				118.5	113.8
$\angle O_{(2)}O_{(1)}O_{(2)}$, deg, exp				116.5[c]	
ω, cm^{-1}	1655 σ_g^+	1181 σ_g^+	691 σ_g^+	754 a_1	438 a_1
				1213 b_2	659 b_2
				1263 a_1	829 a_1
ω_{exp}, cm^{-1}	1580[a]	1145[b]	ca. 770[a]	716	
				1089	
				1135[d]	

[a] Reference 15. [b] Reference 34. [c] Reference 35. [d] Reference 36.

Spin contamination was estimated by calculating the $\langle S^2\rangle$ expectation value, treating the DFT orbitals as single-determinant one-electron wave functions. For most of the low-energy states of CoO_n, the $\langle S^2\rangle$ value did not exceed $M(M+1)$ by more than 0.03.

Cobalt Ions and the Oxygen Species

To gain insight of the reliability of the method and the basis functions employed, we calculated the first three ionization potentials and the electronic states of cobalt cations. The results obtained are in good agreement with experimental data.[34]

$$\begin{bmatrix} Co\ (^4F, 3d^7 4s^2) \rightarrow Co^+\ (^3F) & IP_{calc} = 7.52\ eV & IP_{exp} = 7.86\ eV \\ Co^+\ (^3F) \rightarrow Co^{2+}\ (^4F) & IP_{calc} = 17.42\ eV & IP_{exp} = 17.05\ eV \\ Co^{2+}\ (^4F) \rightarrow Co^{3+}\ (^5D) & IP_{calc} = 34.07\ eV & IP_{exp} = 33.49\ eV \end{bmatrix}$$

Calculated bond lengths and vibrational frequencies compare well with experimental data for the neutral dioxygen molecule, the peroxide and superoxide ion, the ozone molecule, and the ozonide cation; see Table 1. This also holds for the zero-point-corrected oxygen−oxygen bond dissociation energy $D = 4.80$ eV, compared with experimental 5.12 eV,[15] and the zero-point-corrected adiabatic electron affinity of the oxygen molecule $A_{ad} = 0.435$ eV, compared with 0.44 eV.[37] D and A_{ad} are defined as follows:

$$D = E_{tot}(2O) - E_{tot}(O_2) - ZPE(O_2) = D_0 - ZPE(O_2)$$

$$A_{ad} = E_{tot}(O_2) + ZPE(O_2) - E_{tot}(O_2^-) - ZPE(O_2^-)$$

where E_{tot} = total energy and ZPE = zero-point vibrational energy.

The results obtained suggest that both the method (B1LYP) and the basis (6-311+G*) yield results that are in agreement with the experimental data and the calculations could be reliably extended to more complicated cobalt oxide species for which experimental data are scarce.

CoO Molecule and CoO− Anion

The neutral and anionic CoO species ($C_{\infty v}$ symmetry) with equilibrium internuclear distance, calculated for different electronic states are ordered in Figure 1 as to their relative energies. The electronic structure parameters of these species are summarized in Tables 2 and 3. Both B1LYP and CCSD(T) gave the CoO ground state as $^4\Delta$, in agreement with previous assignments.[38] It should be noted that this is not the highest spin state. There is another closely lying quartet state with slightly shorter Co−O bond length and different spatial symmetry of the wave function, $^4\Sigma^-$. For the $^4\Delta$ state the calculated vibrational frequency (885 cm^{-1}) agrees well with the experimental value for the gas phase (852 cm^{-1}).[16] The calculated adiabatic electron affinity for CoO is in excellent agreement with the experimental value;[39] see Table 4.

The ground state of the anion CoO^- is also a high-spin state, $^5\Delta$. Previous theoretical studies pointed to $^3\Sigma^-$ as the ground state for the anion. [14] We have found that the $^5\Delta$ state, with a slightly longer cobalt−oxygen bond length, is more stable than the $^3\Sigma^-$ state by about 0.4 eV. The two triplet states $^3\Sigma^-$ and $^3\Delta$ are closely spaced in energy, but they differ as to their bond lengths; see Table 3. This is reflected in their ν_{Co-O} frequencies.

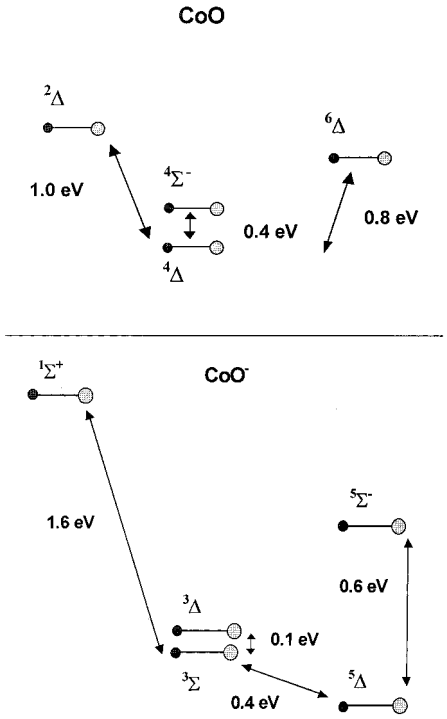

Figure 1. Local and global minima of CoO and CoO^- clusters, ordered as to their relative energies and grouped according to spin multiplicity. The arrows (not to scale) denote the energy difference ΔE_{tot}, corresponding to adiabatic transitions.

TABLE 2: Bond Lengths, Energies, Vibrational Frequencies and Electronic Structure Parameters for CoO[a]

	state			
	$^2\Delta$	$^4\Delta$	$^4\Sigma^-$	$^6\Delta$
R_{Co-O}, Å	1.734	1.629	1.597	1.667
$\Delta E_{tot} \times 10^3$, Hartree				
B1LYP	37.12	0.00	13.42	29.61
(CCSD(T))		(0.00)	(10.61)	
$\langle S^2\rangle$	1.543	3.865	3.766	8.772
ZPE, kJ mol^{-1}	3.45	5.29	5.46	4.60
ω, cm^{-1}	576 σ^+	885 σ^+ (118)	913 σ^+	769 σ^+
DM, Debye	4.85	4.86	5.49	1.66
ESD_{Co}	1.85	2.14	2.33	3.80
ESD_O	−0.85	0.86	0.67	1.20
q_{Co}	0.41	0.42	0.48	0.29
q_O	−0.41	−0.42	−0.48	−0.29

[a] CCSD(T) energy values with respect to the B1LYP optimized geometries are given in parentheses. ΔE_{tot} is the total energy difference relative to the ground state: $E_{tot} = -1457.88038$ Hartree for B1LYP, −1456.58615 for CCSD(T); 1 Hartree = 2625.499748 kJ mol^{-1}. $\langle S^2\rangle$ is the spin contamination expectation value. ZPE is the zero-point energy. ω is the harmonic vibrational frequencies; symmetry modes are given after the wavenumbers. IR intensities in km mol^{-1} for the ground state are given in parentheses. DM is the dipole moment. ESD is electron spin density. q is the atomic charge.

TABLE 3: Bond Lengths, Energies, Harmonic Vibrational Frequencies, and Electronic Structure Parameters for CoO^- [a]

	state				
	$^1\Sigma^+$	$^3\Sigma^-$	$^3\Delta$	$^5\Delta$	$^5\Sigma^-$
R_{Co-O}, Å	1.604	1.632	1.698	1.685	1.665
$\Delta E_{tot} \times 10^3$, Hartree					
B1LYP	73.33	13.29	15.89	0.00	20.32
(CCSD(T))		(20.10)		(0.00)	
$\langle S^2 \rangle$	0.000	2.560	3.014	6.032	6.011
ZPE, kJ mol^{-1}	5.31	5.02	4.61	4.76	4.95
ω, cm^{-1}	888 σ^+	840 σ^+	770 σ^+	796 σ^+ (218)	828 σ^+
DM, Debye	1.67	2.22	1.02	1.08	1.56
ESD_{Co}	0.00	1.58	1.72	3.20	3.36
ESD_O	0.00	0.42	0.28	0.80	0.64
q_{Co}	−0.26	−0.20	−0.24	−0.28	−0.19
q_O	−0.74	−0.80	−0.76	−0.72	−0.81

[a] Notations as in Table 2. ΔE_{tot} is the total energy difference relative to the ground state: $E_{tot} = -1457.93298$ Hartree for B1LYP, −1456.64079 for CCSD(T).

The $^3\Delta$ state has the same spatial symmetry as the ground $^5\Delta$ state and through mixing with the higher spin state may lower its energy, thus pushing $^3\Delta$ below $^3\Sigma^-$. $\langle S^2 \rangle$ values indicate spin contamination for the neutral doublet CoO and for the triplet monoanions; see Tables 2 and 3. CCSD(T) calculations confirmed the ordering of the lowest energy states. The energy gap between the quintet and triplet CoO^- determined by B1LYP was lower than the value obtained with CCSD(T). All excited states are thermally inaccessible since the energy differences are much higher than $^3/_2KT \approx 300$ cm^{-1}.

The results for CoO compared with those for CoO^- show that the anions are more stable than the parent neutral species. There is a slight lengthening of the Co−O bond on going from CoO to CoO^-. Concurrently, the calculated vibrational frequencies decrease by about 90 cm^{-1}. High electron spin density is present on the oxygen atom in both the neutral molecule and the anion. In the doublet configuration, antiferromagnetic coupling between the two centers is observed.

CoO_2 Molecule and CoO_2^- Anion

Potential Energy Surfaces (PES). The experimental data of several authors[17,18] show that CoO_2 in solid-state matrixes is linear in a doublet state. This finding prompted us to study in detail the $^2A_1$ state, which is the lowest energy doublet of CoO_2 with bent geometry; see Figure 2. The $^2\Sigma_g^+$ doublet state of the linear CoO_2 molecule is a first-order saddle point (transition state) on the path connecting the two symmetrically located bent $^2A_1$ configurations of CoO_2 with $\angle OCoO = 156.5°$ and $\angle OCoO = 2\pi - 156.5°$, passing through a narrow valley; see Figure 3. The linear transition state was recognized by a degenerate imaginary vibration π_u (−89 cm^{-1}) and one negative eigenvalue in the force constant matrix. The energy gap between the occupied σ_u (lower than the HOMO) and the π_g (LUMO) is 5.22 eV. The instability of the linear molecule in terms of the second-order Jahn−Teller effect is expected to be small because of the high energy gap. It should be manifested by a transition electron density $\Gamma = \sigma_u \times \pi_g = \pi_u$.[40,41] Amplitude motions corresponding to the imaginary vibration π_u should take the linear CoO_2 molecule to one of the symmetrically located potential energy minima with bent geometry through vibroelectronic interaction. According to B1LYP results, the energy,

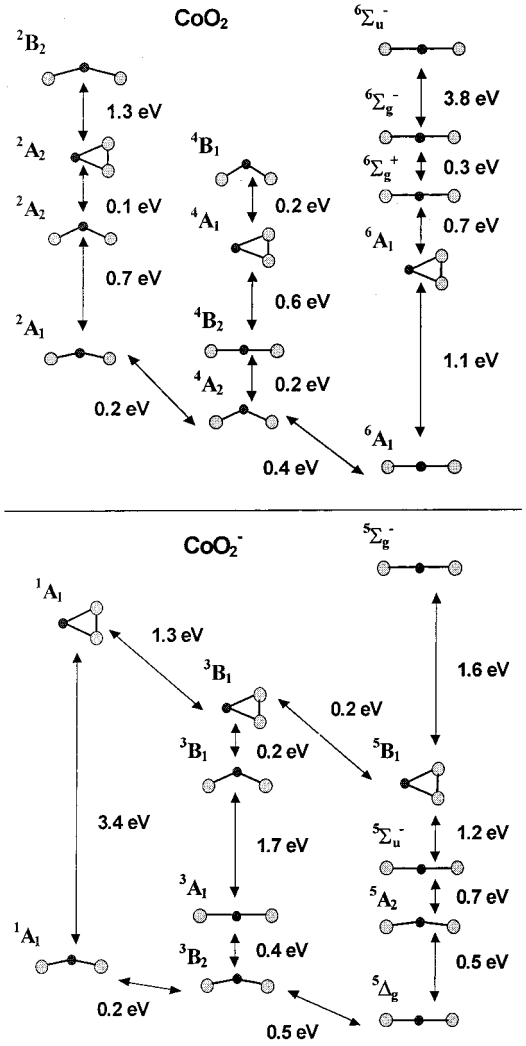

Figure 2. Local and global minima of CoO_2 and CoO_2^- clusters, corresponding to peroxides and oxides, ordered as to their relative energies and grouped according to spin multiplicity. The arrows (not to scale) denote the energy difference ΔE_{tot}, corresponding to adiabatic transitions.

TABLE 4: Adiabatic Electron Affinities (A_{ad}), HOMO−LUMO Energy Gaps of CoO_n, and Vertical Detachment Energies (E_{vd}) of the Corresponding Anions

	CoO $^4\Delta$	CoO_2 $^4A_2$ bent oxide	CoO_2 $^6A_1$ quasilinear oxide	$Co(O_2)$ $^6A_1$ peroxide	CoO_3 $^4A_2$ oxoperoxide	CoO_3 $^6A_1$ oxoperoxide	CoO_4 $^6B_2$ peroxide
A_{ad}, eV[a]	1.44	3.03	3.11	1.74	2.68	2.66	3.02
A_{ad}, eV, exp	1.45[c]	-	2.97[d]	-	-	-	-
HOMO−LUMO, eV	3.07	3.35	3.30	2.50	3.45	3.81	3.70
	CoO^- $^5\Delta$	CoO_2^- $^3B_2$	CoO_2^- $^5\Delta_g$	CoO_2^- $^5B_1$	CoO_3^- $^3B_2$	CoO_3^- $^5A_1$	CoO_4^- $^6B_2$
E_{vd}, eV[b]	1.87	3.74	4.44	-	3.66	4.28	4.87

[a] Zero-point corrections are included. [b] $E_{vd} = E_{tot}^{neutral}(R^{anion}) - E_{tot}^{anion}(R^{anion})$. [c] Reference 39. [d] Cited in ref 7.

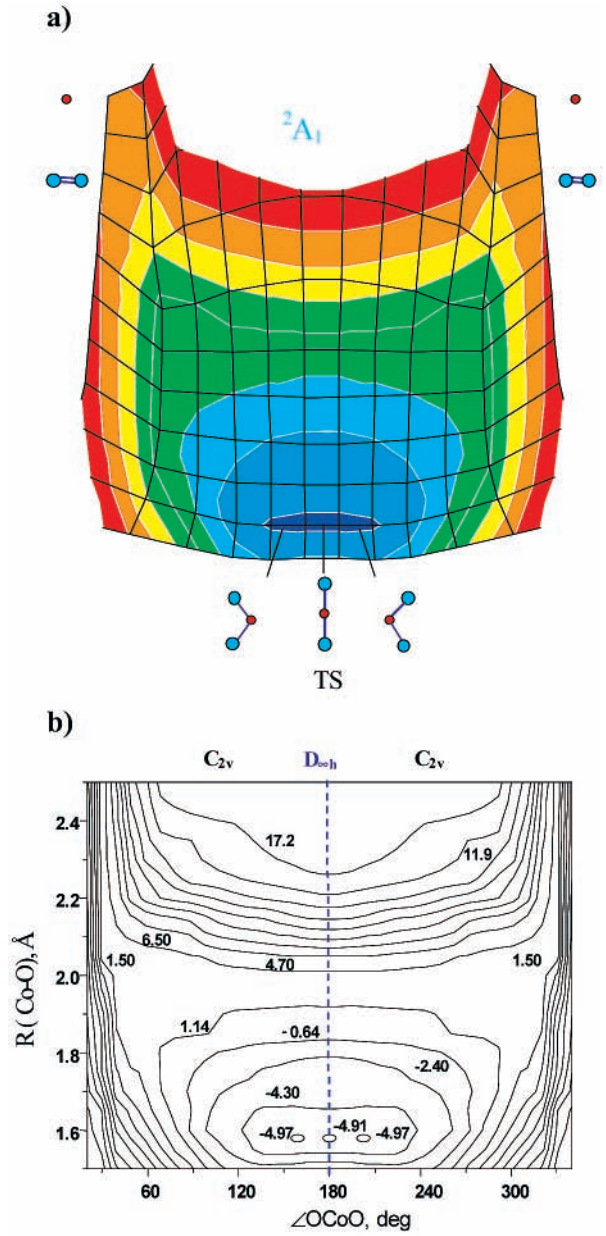

Figure 3. (a) Potential energy surface of CoO_2 in its $^2A_1$ state. The local minima, the linear transition state, and the dissociation products are denoted. (b) Contour diagram of CoO_2 in its $^2A_1$ state as a function of the internal coordinates R_{Co-O} and ∠OCoO. Energy values are scaled $(E_{tot} + 1533) \times 10^2$ Hartree.

required for reaching the linear configuration is only 150 cm^{-1}. Hence, the two physically equivalent bent CoO_2 molecules in the $^2A_1$ state may oscillate between the two minima, giving an averaged linear structure; see Scheme 1. The transition state linear doublet is of much higher energy with the CCSD(T) method than with B1LYP, Table 5. It should be noted that the CCSD(T) calculations failed to converge for the $^2A_1$ and $^4A_2$ states with B1LYP-produced geometries. In the region of small angles and large internuclear Co−O distances of the $^2A_1$ PES, a narrow dissociation path leads to Co + O_2.

The potential energy surfaces of the $^6A_1$ and the $^2A_1$ states of CoO_2 do not cross on bending the molecule. However, the $^2A_1$ and $^2A_2$ states do intersect at OCoO angles corresponding to the peroxide structure. It should be noted that the $^2A_1$ state has no minimum that corresponds to a peroxide structure. The doublet peroxide configuration has A_2 symmetry; see Figure 2. The $^6A_1$ minima correspond to a quasilinear oxide, which is the ground state, and to peroxide; see Figure 4. The peroxide may easily decompose to Co + O_2 along a narrow path with a relatively low-energy barrier of 1.5 eV. The energy difference between the oxide and peroxide sextet states was nearly the same with B1LYP and CCSD(T). Thus, the $^6A_1$ PES may be considered as "soft".

Oxides, CoO_2, and CoO_2^-. The oxides exist in $D_{\infty h}$ (linear) and C_{2v} (bent and quasilinear symmetry), as seen from Figure 2. The valence 3d, 4s, 4p AOs of Co and the 2s, 2p AOs of the two oxygen atoms span the $7a_1 + 2a_2 + 3b_1 + 5b_2$ MOs in C_{2v} symmetry (the molecule lying in the *yz* plane and $C_2 \equiv z$, as oriented by Gaussian) and $4\sigma_g^+ + 2\pi_g + \delta_g + 3\sigma_u^+ + 2\pi_u$ MOs in $D_{\infty h}$ symmetry (the molecule lying along the *z*-axis). The CoO_2 ground state is $^6A_1$ with quasilinear geometry. The HOMO is an oxygen nonbonding b_1-MO and the HOMO−LUMO energy gap is higher than in cobalt monoxide; see Table 4. Cobalt−oxygen bonds are shorter in the linear $^6\Sigma_g^+$ state CoO_2 than in the ground-state CoO_2; see Table 5. The energy gap between the π_u(HOMO) and the unoccupied σ_g MO (higher than the LUMO) for the $^6\Sigma_g^+$ dioxide is 2.27 eV. This value is lower than the HOMO−LUMO gap for the quasilinear oxide and the peroxide and can lead to instability. No minimum was detected for a bent oxide in the sextet state and there is an energy barrier to the formation of the peroxide in its $^6A_1$ state. The $D_{\infty h}$ symmetry of the ground state is lowered to C_{2v} and the resulting global minimum corresponds to a quasilinear structure with $^6A_1$ state. Quasilinear geometry was also determined for the quartet state $^4B_2$ of CoO_2 and the triplet state anion $^3A_1$; see Table 6. The CoO_2 clusters in the $^2B_2$, $^6\Sigma_u^-$, and $^6\Sigma_g^-$ states are thermodynamically unstable. The reaction paths with release of molecular oxygen are exothermic. The energy of the $^2B_2$ state is also close to that of the dissociation products CoO + O, requiring 0.4 eV to reach the dissociation limit. The linear CoO_2 in the $^6\Sigma_u^-$ state readily dissociates one oxygen atom with an energy gain of 2.7 eV, which exceeds by 1 eV the energy needed for the release of a second oxygen atom.

The quasilinear cobalt dioxide readily accepts one electron to form an anion. When an electron is attached adiabatically, the nature of the parent MOs is changed and the number of nonbonding MOs is reduced. This stabilizes further the anion in linear geometry with $^5\Delta_g$ ground state. It should be noted that the adiabatic electron affinity of CoO_2 is the highest among the CoO_n ($n = 1-4$) species, due to the high stability of this monoanion; see Table 4. Similar to the monoxide anions, spin contamination is the highest for the dioxide and peroxide monoanions in their triplet states; see Table 6. The CCSD(T) calculations for the lowest energy anions are in agreement with the B1LYP values and confirm the ordering of states.

Peroxides, $Co(O_2)$, and $Co(O_2)^-$. The relative stability of both the neutral and the anion peroxide species increases with increasing spin multiplicity. The O−O bond length in cobalt peroxides is shorter than the value for the free peroxide anion (1.49 Å); see Tables 5 and 6. It should be noted that the cobalt−oxygen bond length in the peroxides is much longer (1.8−2.0 Å) than in the dioxides (1.5−1.9 Å) and that in general the cobalt−oxygen bond length in the sextet states is always longer than in the quartet and doublet states. The three uncharged peroxide species listed in Figure 2 and Table 5 have a very small OCoO angle (38−46°), once again the lowest value (37.8°) being related to the sextet state. The dioxides in this state are invariably linear.

Comparing the bond lengths and bond angles on going from $Co(O_2)$ to $Co(O_2)^-$ reveals the following tendencies: (i) The O−O bond length increases by about 0.08 Å for the lowest spin

TABLE 5: Bond Lengths, Bond Angles, and Energies for CoO_2[a]

cluster model	state	R_{Co-O}, Å	R_{O-O},[b] Å	∠OCoO, deg	$\langle S^2 \rangle$	$\Delta E_{tot} \times 10^3$, Hartree B1LYP (CCSD(T))
oxide, quasilinear	$^6A_1$	1.745		179.9	8.775	0.00 (0.00)
(C_{2v})	$^4B_2$	1.639		179.9	3.973	19.95
oxide, linear	$^6\Sigma_g^+$	1.701		180.0	8.804	65.92
($D_{\infty h}$)	$^6\Sigma_g^-$	1.795		180.0	8.782	76.74
	$^6\Sigma_u^-$	1.928		180.0	8.842	216.44
TS ($D_{\infty h}$)	$^2\Sigma_g^+$	1.573		180.0	0.856	22.7 (65.9)
oxide, bent	$^4A_2$	1.605		132.6	3.822	13.39
(C_{2v})	$^2A_1$	1.565		156.5	0.818	22.06
	$^2A_2$	1.572		148.3	0.770	47.27
	$^4B_1$	1.656		100.9	3.792	50.62
	$^2B_2$	1.618		157.9	0.852	100.55
peroxide	$^6A_1$	2.028	1.315	37.8	8.764	41.54 (41.50)
(C_{2v})	$^4A_1$	1.835	1.425	45.7	3.866	42.26
	$^2A_2$	1.837	1.371	43.8	1.274	52.00

cluster model	state	R_{Co-O}, Å	R_{O-O},[c] Å	∠CoOO, deg	$\langle S^2 \rangle$	$\Delta E_{tot} \times 10^3$ Hartree B1LYP
superoxide	$^2A'$	1.863	1.303	115.2	1.774	41.34
(C_s)	$^4A'$	1.894	1.309	110.0	4.106	44.40
	$^4A''$	1.784	1.332	119.8	3.762	54.53

[a] ΔE_{tot} is the total energy difference relative to the ground state: $E_{tot} = -1533.07178$ Hartree for B1LYP, -1531.63002 for CCSD(T); CCSD(T) values are given in parentheses. [b] O−O distance in peroxide. [c] O−O distance in superoxide.

SCHEME 1: Vibroelectronic Interaction of the $^2\Sigma_g^+$ State with the π_u Vibrational Mode in Linear CoO_2[a]

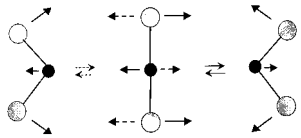

[a] The arrows represent the two degenerate π_u vibrations that take the linear molecule into one of the two symmetrically located minima of the bent CoO_2.

states; however, it increases by 0.18 Å for the highest spin state and reaches 1.4−1.5 Å, a value that is typical for a single O−O bond. (ii) The cobalt−oxygen bond length shows complicated variance: it decreases for the lowest and highest spin states but increases slightly for the quartet−triplet states. (iii) The OCoO angle increases for all the three pairs doublet−singlet, quartet−triplet, and sextet−quintet states.

The electron spin density on the cobalt atom is higher for peroxides than for dioxides; see Table 7. The electron, attached to the neutral molecule is delocalized over the cation center and the oxygen atoms, resulting in a redistribution of the electron spin density and the partial atomic charges. The adiabatic electron affinities of the peroxides are much smaller compared to those of the dioxides; see Table 4.

Superoxides, CoOO. Their stability is similar to that of the peroxides; Table 5. However, unlike the dioxides and peroxides, the doublet state $^2A'$ for CoOO is the most stable. It is seen from Table 5 that the cobalt−oxygen bond length in superoxides is 1.8−1.9 Å, comparable to that in peroxides, but much longer (by 0.2−0.3 Å) than in dioxides. Another feature worth mentioning is that the three superoxide states have bent geometry, the CoOO angle being 110−120°. The middle oxygen atom forms a partial double bond to the terminal oxygen atom: the O−O bond length in the superoxides is 1.30−1.33 Å, which is midway between a double O═O bond (1.21 Å) and a single O−O bond (1.45 Å). [15] A two-step dissociation of peroxides may easily occur with breaking one Co−O bond to form the superoxides, followed by release of molecular oxygen.

Electron spin density over the transition metal atom is even higher than in peroxides and much higher, than in oxides; see Table 7. The terminal oxygen atom has higher electron spin density than the other oxygen atom, but with a smaller negative charge. Spin contamination is significant for the $^2A'$ and $^4A'$ states of the superoxides; see Table 5.

Vibrational Modes. The irreducible representation of the symmetry modes, spanned by bent CoO_2 clusters is $\Gamma = 2a_1(IR,R) + b_2(IR,R)$ and for the linear oxides $\Gamma = \sigma_g^+(R) + \sigma_u^+(IR) + \pi_u(IR)$. The two a_1-modes correspond to Co−O symmetric stretch and CoO_2 bending; the b_2-mode is a Co−O antisymmetric stretching vibration. In peroxides, one of the a_1-bending modes at high frequency is expected to appear with the highest intensity in the IR spectrum; this mode represents an oxygen−oxygen stretching. Comparison of the vibrational modes of oxides and peroxides reveals that a_1-modes in peroxides are at higher energy, while the b_2-mode is at lower energy, Table 7. For bent and quasilinear oxides, the b_2-mode is at high frequency and with high intensity. The quasilinear oxide in its ground state is an exception, the a_1-bending mode being most intensive but located at lower energy in the IR spectrum. For linear CoO_2 oxides, the σ_u^+-antisymmetric stretching mode is at higher frequency and with higher intensity in the IR spectrum than the π_u-bending mode. In superoxides CoOO, where the three vibrational modes have a′ symmetry, the highest frequency vibration represents an oxygen−oxygen stretching mode.

CoO_3 Molecule and CoO_3^- Anion

Oxides, CoO_3, and CoO_3^-. The three doublet states that arise from the trioxide structures were found to be thermodynamically unstable with respect to CoO + O_2 dissociation. It should be noted that all the three doublet states are of C_{2v} instead of D_{3h} symmetry with one longer and two shorter Co−O bonds; see Table 8. No minima were detected for the highest symmetry structure D_{3h}; see Tables 8 and 9. The OCoO angle, composed of the shorter Co−O bonds, is larger (128−152°) than the 120° value defined by the D_{3h} structure, thus displaying avoided repulsion between the oxygen atoms. Attachment of an electron to the trioxides does not stabilize the structure and no minimum corresponding to trioxide could be found for the anions in singlet and triplet states; see Figure 5. While the calculated energies of uncharged oxides are above the dissociation limit, the anion

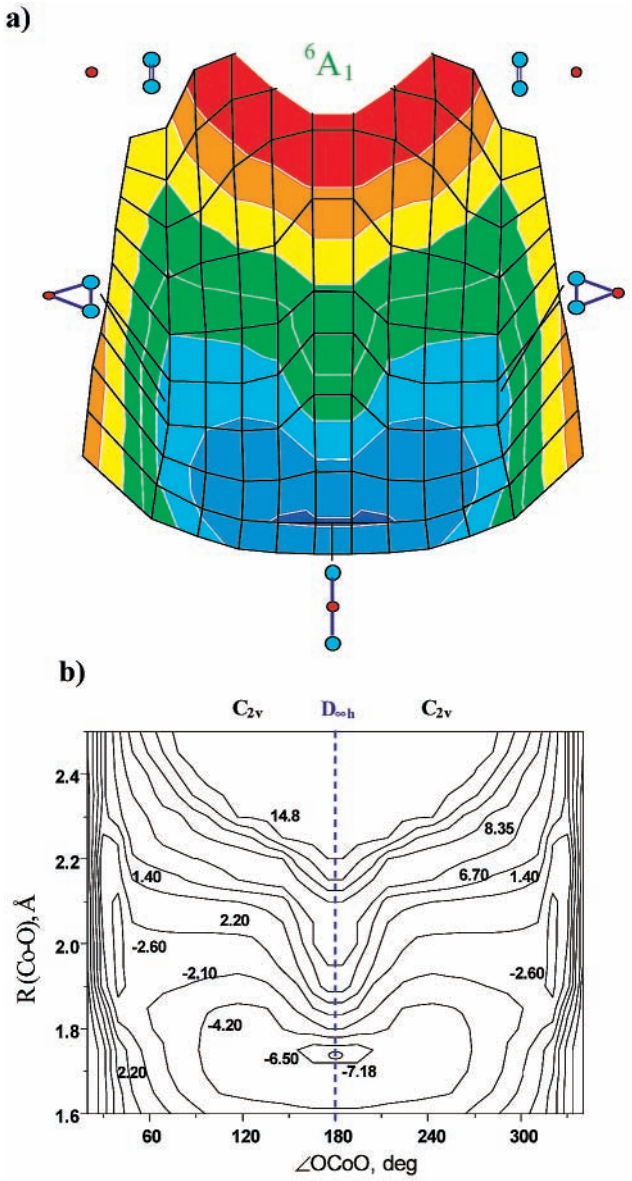

Figure 4. (a) Potential energy surface of CoO_2 in its $^6A_1$ state. The local minima and the dissociation products are denoted. The ground state is quasilinear, ∠OCoO = 179.9°. (b) Contour diagram of CoO_2 in its $^6A_1$ state as a function of the internal coordinates R_{Co-O} and ∠OCoO. Energy values are scaled $(E_{tot} + 1533) \times 10^2$ Hartree.

in its ground state $^5A_1$ is a thermodynamically stable oxide. The next state of the monoanion has the oxoperoxide structure.

Oxoperoxides $OCo(O_2)$ and $OCo(O_2)^-$. The calculated states of oxoperoxides are thermodynamically stable with respect to dissociation. The O−O bond length in the $OCo(O_2)$ oxoperoxides is shorter than that in the $Co(O_2)$ peroxides. This is also valid for the monoanions; see Tables 8 and 9 and indicates that the O−O bond length in the oxoperoxides still preserves a partial double bond nature. The electron spin density at the axial oxygen atom correspnds to one unpaired electron; see Table 10. In the quartet states, the unpaired electrons at the cobalt center and the two equivalent peroxide oxygen atoms are antiferromagnetically coupled. Figure 5 shows that neutral oxoperoxides occupy the lowest energy part of the diagram, the $^6A_1$ state being the ground state. It should be noted that this state spans one of the lowest frequency vibrations (62 cm^{-1}). Unlike the trioxides with one longer and two shorter CoO bonds, the oxoperoxides show the reverse picture—two much longer Co−O bonds (ca. 2.0 Å) that form the triatomic CoO_2 ring and one shorter CoO bond (1.7−1.8 Å) that lies on the C_2 axis. The OCoO angle in the ring is much smaller than the same angle in peroxides $Co(O_2)$. The geometry of $OCo(O_2)$ in its ground state is very similar to that of the lower multiplicity state $^4A_2$ and the energy differs only by 950 cm^{-1}, which allows spin-state flipping. The HOMO−LUMO energy gaps are the largest for these configurations, compared to those of the ground states of CoO and CoO_2; see Table 4. The HOMO of $OCo(O_2)$ in the $^6A_1$ ground state has b_2 symmetry with major contribution of nonbonding O 2p orbitals.

Oxoperoxide anions are stable in their lower multiplicity states, $^1A_1$ and $^3B_2$; see Table 9. The ground state of the trioxide anion with $^5A_1$ symmetry is by 0.1 eV lower in energy than the $^3B_2$ state of the oxoperoxide. The geometry of the two anions is, however, rather different. An extra electron to the oxoperoxide in its $^6A_1$ ground state leading to the lower multiplicity state $^5A_1$ results in breaking the O−O bond and shortening of the two equivalent Co−O bonds. Attachment of an electron to the oxoperoxide in its $^4A_2$ state may occur in two ways; see Figure 5: (a) resulting in a trioxide anion as global minimum and (b) resulting in an oxoperoxide anion as local minimum with lower multiplicity in $^3B_2$ state. In the latter case the O−O bond is elongated by 0.086 Å and the two equivalent Co−O bonds are shortened by 0.157 Å. The adiabatic electron affinity and the vertical detachment energy involving the neutral oxoperoxide's ground state and the trioxide anion's ground state vary considerably, because of the rather different geometry of these states; see Table 4. For the CoO_3 and CoO_3^- low-energy states, coupled-cluster calculations yielded energy differences slightly larger than B1LYP. Spin contamination was the lowest for the high-spin states; see Tables 8 and 9.

TABLE 6: Bond Lengths, Bond Angles, and Energies for CoO_2^- [a]

cluster model	state	R_{Co-O}, Å	R_{O-O},[b] Å	∠OCoO, deg	$\langle S^2 \rangle$	$\Delta E_{tot} \times 10^3$ Hartree B1LYP (CCSD(T))
oxide, linear	$^5\Delta_g$	1.689		180.0	6.041	0.00 (0.00)
($D_{\infty h}$)	$^5\Sigma_u^-$	1.725		180.0	6.021	66.20
	$^5\Sigma_g^-$	1.839		180.0	6.115	153.72
oxide, quasilinear	$^3A_1$	1.677		179.9	3.049	31.15
oxide, bent	$^3B_2$	1.663		149.6	2.245	17.36 (16.02)
(C_2v)	$^1A_1$	1.606		167.2	0.000	25.29
	$^5A_2$	1.742		165.0	6.101	48.80
	$^5B_2$	1.741		165.6	6.101	48.83
	$^3B_1$	1.697		131.6	2.127	94.45
peroxide	$^1A_1$	1.803	1.451	47.5	0.000	150.07 (132.69)
(C_2v)	$^3B_1$	1.877	1.486	46.6	2.934	100.31
	$^5B_1$	1.889	1.484	46.3	6.011	93.49

[a] ΔE_{tot} is the total energy difference relative to the ground state: $E_{tot} = -1533.18717$ Hartree for B1LYP, −1531.74876 for CCSD(T); CCSD(T) values are given in parentheses. [b] O−O distance in peroxide.

TABLE 7: Vibrational Frequencies and Electronic Structure Parameters for CoO_2 and CoO_2^- [a]

	CoO_2					
	state					
	$^4B_2$ oxide quasilinear	$^4A_1$ peroxide	$^6A_1$ oxide quasilinear	$^6A_1$ peroxide	$^6\Sigma_g^+$ oxide	$^2A'$ superoxide
ω, cm^{-1}	121 a_1	311 a_1	184 a_1 (41)	308 b_2 (6)	242 π_u	197 a′ (8)
	784 a_1	323 b_2	528 b_2 (18)	383 a_1 (25)	692 σ_g^+	472 a′ (5)
	1053 b_2	898 a_1	635 a_1 (0)	1176 a_1 (105)	730 σ_u^+	1123 a′ (593)
ZPE, kJ mol^{-1}	11.71	9.16	8.05	11.16	11.40	10.72
DM, Debye	0.00	6.16	0.00	1.59	0.00	4.87
ESD_{Co}	2.90	2.12	2.80	3.67	3.22	2.11
ESD_O	0.05	0.44	1.10	0.66	0.89	−0.40
						−0.72[b]
q_{Co}	0.55	0.54	0.55	0.26	0.58	0.40
q_O	−0.28	−0.27	−0.27	−0.13	−0.29	−0.25
						−0.15[b]

	CoO_2^-					
	state					
	$^1A_1$ oxide	$^3B_2$ oxide	$^3A_1$ oxide quasilinear	$^5A_2$ oxide	$^5B_1$ peroxide	$^5\Delta_g$ oxide
ω, cm^{-1}	70 a_1	98 a_1	146 a_1	60 a_1	392 b_2 (29)	134 π_u (85)
	869 a_1	707 a_1	773 a_1	628 a_1	496 a_1 (52)	758 σ_g^+
	1037 b_2	1369 b_2	844 b_2	748 b_2	830 a_1 (116)	859 σ_u^+ (345)
ZPE, kJ mol^{-1}	11.82	13.01	10.54	8.59	10.28	11.27
DM, Debye	0.39	1.53	0.00	0.26	1.86	0.00
ESD_{Co}	0.00	2.13	0.82	2.27	3.52	2.86
ESD_O	0.00	−0.06	0.59	0.86	0.24	0.57
q_{Co}	0.11	0.21	0.28	0.17	−0.05	0.31
q_O	−0.56	−0.60	−0.64	−0.58	−0.47	−0.65

[a] Notations as in Table 2. IR intensities in km mol^{-1} for the low energy states given in parentheses. [b] Values for the terminal oxygen atom in cobalt superoxide.

TABLE 8: Bond Lengths, Bond Angles, and Energies for CoO_3[a]

cluster model	state	$R_{Co-O(1)}$,[b] Å	$R_{Co-O(2)}$,[b] Å	R_{O-O}, Å	$\angle O_{(2)}CoO_{(2)}$, deg	$\angle O_{(2)}O_{(1)}O_{(2)}$, deg	$\langle S^2\rangle$	$\Delta E_{tot} \times 10^3$ Hartree B1LYP (CCSD(T))
oxoperoxide	$^6A_1$	1.653	1.984	1.329	39.1		8.780	0.00 (0.00)
(C_{2v})	$^6A_2$	1.652	2.00	1.325	38.6		8.780	2.13 (3.41)
	$^4A_2$	1.659	1.984	1.329	39.1		4.742	4.29 (5.60)
	$^6B_2$	1.837	1.962	1.316	39.2		8.781	25.18
	$^4B_1$	1.846	1.963	1.321	39.3		4.739	32.62
oxide	$^2B_1$	1.623	1.555		128.0		0.781	54.46
(C_{2v})	$^2B_2$	1.785	1.548		139.5		0.833	82.81
	$^2A_1$	1.750	1.618		152.5		1.846	105.48
ozonide	$^4A_1$	2.359	1.846	1.426	74.4	103.0	3.766	53.89
(C_{2v})	$^2A_1$	2.577	2.128	1.342	62.7	111.1	1.733	78.16
	$^6A_1$	2.529	2.058	1.348	64.2	108.5	8.759	79.86

cluster model	state	$R_{Co-O(1)}$,[b] Å	$R_{Co-O(2)}$,[b] Å	R_{O-O}, Å	∠CoOO, deg	∠OCoO, deg	$\langle S^2\rangle$	$\Delta E_{tot} \times 10^3$ Hartree B1LYP
oxosuperoxide (C_s)	$^6A'$	1.647	1.836	1.283	146.2	164.5	8.783	21.43

[a] ΔE_{tot} is the total energy difference relative to the ground state: $E_{tot} = -1608.25820$ Hartree for B1LYP, −1606.67961 Hartree for CCSD(T); CCSD(T) values given in parentheses. [b] In oxoperoxides and ozonides, (1) refers to oxygen atoms, positioned along the C_2 axis and (2) refers to the other two oxygen atoms in the σ_v plane; in oxosuperoxides, O(1), O(2), and O(3) represent the nonequivalent oxygen atoms: O(1)−Co−O(2)−O(3).

Oxosuperoxides, OCoOO. The lowest energy oxosuperoxide with C_s symmetry is in high spin state $^6A'$, in agreement with previous studies;[7] see Table 8. The energy of this $^6A'$ state is 0.6 eV higher than that of the oxoperoxide's ground state. The O−O and the Co−O_s (s = superoxide oxygen) bond lengths in the oxosuperoxide are shorter than in the oxoperoxides. Electron spin density at the two terminal oxygen atoms corresponds approximately to one unpaired electron per oxygen atom; see Table 10.

Ozonides $Co(O_3)$ and $Co(O_3)^-$. The ozonides are planar cyclic clusters with C_{2v} symmetry. They occupy the high-energy part of the diagram; see Figure 5. The neutral clusters are unstable toward dissociation with release of molecular dioxygen, although their energies are lower compared to those of the neutral oxide structures. The ozonide anions are more stable than their neutral parent species, Tables 8 and 9. Cobalt ozonides have lower electron spin density at the oxygen atoms than the oxides and oxoperoxides. The doublet state is an exception to

TABLE 9: Bond Lengths, Bond Angles, and Energies for CoO_3^- [a]

cluster model	state	$R_{Co-O(1)}$,[b] Å	$R_{Co-O(2)}$,[b] Å	R_{O-O}, Å	$\angle O_{(2)}CoO_{(2)}$, deg	$\angle O_{(2)}O_{(1)}O_{(2)}$, deg	$\langle S^2 \rangle$	$\Delta E_{tot} \times 10^3$ Hartree B1LYP (CCSD(T))
oxide (C_{2v})	$^5A_1$	1.653	1.699		91.1		6.047	0.00 (0.00)
oxoperoxide	$^3B_2$	1.665	1.827	1.415	45.6		2.131	2.70 (2.96)
(C_{2v})	$^5A_1$	1.678	2.056	1.344	38.14		6.049	7.98
	$^1A_1$	1.625	1.854	1.439	45.7		0.000	73.05
ozonide	$^5A_1$	2.455	1.911	1.450	72.3	102.0	6.010	85.82
(C_{2v})	$^3B_2$	2.632	2.171	1.348	61.4	110.7	2.986	126.90

[a] ΔE_{tot} is the total energy difference relative to the ground state: $E_{tot} = -1608.35559$ Hartree for B1LYP, -1606.71579 Hartree for CCSD(T); CCSD(T) values given in parentheses. [b] (1) refers to oxygen atoms, positioned along the C_2 axis, and notation (2) refers to the other two oxygen atoms in the σ_v plane.

TABLE 10: Vibrational Frequencies and Electronic Structure Parameters for CoO_3 and CoO_3^- [a]

CoO_3

	state			
	$^4A_2$ oxoperoxide	$^4A_1$ ozonide	$^6A_1$ oxoperoxide	$^6A'$ oxosuperoxide
ω, cm^{-1}	114 b_1	262 b_1 (8)	62 b_2 (38)	83 a′ (22)
	137 b_2	407 a_1 (0)	142 b_1 (38)	98 a″ (29)
	287 b_2	508 b_2 (29)	324 b_2 (0)	151 a′ (16)
	441 a_1	742 a_1 (2)	428 a_1 (13)	462 a′ (4)
	654 a_1	752 b_2 (85)	715 a_1 (24)	743 a′ (25)
	1172 a_1	821 a_1 (108)	1161 a_1 (83)	1194 a′ (503)
ZPE, kJ mol^{-1}	16.77	20.89	16.94	16.33
DM, Debye	0.49	6.27	0.75	0.91
ESD_{Co}	2.77	2.40	2.71	2.71
$ESD_{O(1)}$	1.05	0.07	1.02	0.99
$ESD_{O(2)}$	−0.41	0.27	0.63	0.44
$ESD_{O(3)}$				0.86
q_{Co}	0.59	0.52	0.58	0.60
$q_{O(1)}$	−0.30	−0.08	−0.31	−0.34
$q_{O(2)}$	−0.14	−0.22	−0.13	−0.26
$q_{O(3)}$				0.00

CoO_3^-

	state			
	$^3B_2$ oxoperoxide	$^5A_1$ oxide	$^5A_1$ ozonide	$^5A_1$ oxoperoxide
ω, cm^{-1}	126 b_2	38 b_2 (11)	253 b_1 (1)	106 b_2 (14)
	160 b_1	214 b_1 (31)	426 a_1 (49)	151 b_1 (12)
	469 a_1	250 a_1 (1)	427 b_2 (33)	221 b_2 (0.5)
	504 b_2	555 b_2 (8)	677 a_1 (62)	349 a_1 (26)
	863 a_1	737 a_1 (13)	778 b_2 (13)	836 a_1 (179)
	964 a_1	891 a_1 (197)	879 a_1 (13)	1156 a_1 (29)
ZPE, kJ mol^{-1}	18.46	16.06	20.57	16.87
DM, Debye	1.56	0.21	1.05	3.47
ESD_{Co}	1.93	1.76	3.60	2.31
$ESD_{O(1)}$	0.22	0.47	0.01	0.57
$ESD_{O(2)}$	−0.07	0.89	0.20	0.56
q_{Co}	0.29	0.38	−0.08	0.21
$q_{O(1)}$	−0.65	−0.56	−0.17	−0.71
$q_{O(2)}$	−0.32	−0.41	−0.38	−0.25

[a] Notations as in Table 2; oxygen atoms are indexed as in Table 8. IR intensities in km mol^{-1} for the low-energy states are given in parentheses.

this trend with typical antiferromagnetic interaction between the unpaired electrons of cobalt and oxygen. The most stable ozonide structure has a $^4A_1$ ground state. The HOMO has b_1-symmetry, delocalized over the cobalt atom and the three oxygen atoms; it is a π-bond with the participation of $Co3d_{xz}$ and $O2p_x$ AOs. The unpaired electrons are localized predominantly at the cobalt atom; the same is valid for the lowest-energy ozonide anion in a $^5A_1$ state.

Vibrational Modes. Cobalt oxide clusters CoO_3 (oxides, oxoperoxides, and ozonides) have C_{2v} symmetry. They span the irreducible representation $\Gamma = 3a_1(IR,R) + b_1(IR,R) + 2b_2(IR,R)$. The b_1-mode represents an out-of-plane vibration and appears in the lower energy part of the vibrational spectrum. In oxoperoxides the highest frequency vibration, which is also the most intensive one in the IR spectrum, corresponds to an a_1-symmetry oxygen−oxygen stretching mode. For the oxide monoanion in its ground state, the highest frequency vibration corresponds to a CoO_2 bending mode, coupled to the CoO stretching mode with axial oxygen participation. In ozonides, the a_1-mode, which corresponds to O_3 bending, is at a lower frequency; this vibration appears with the highest IR intensity. The oxosuperoxides span the irreducible representation $\Gamma = 5a'(IR,R) + a''(IR,R)$. The highest frequency vibration is the most intensive one and corresponds to oxygen−oxygen stretching with superoxide oxygen's participation.

CoO_4 Molecule and CoO_4^- Anion

Structure and Energetics. Diperoxides with D_{2d} symmetry are the stable structures, found for the uncharged CoO_4 clusters, Figure 6. The HOMO−LUMO energy gap for the $^6B_2$ ground state (see Table 4) is higher than that for CoO_n ($n = 1, 2$) and

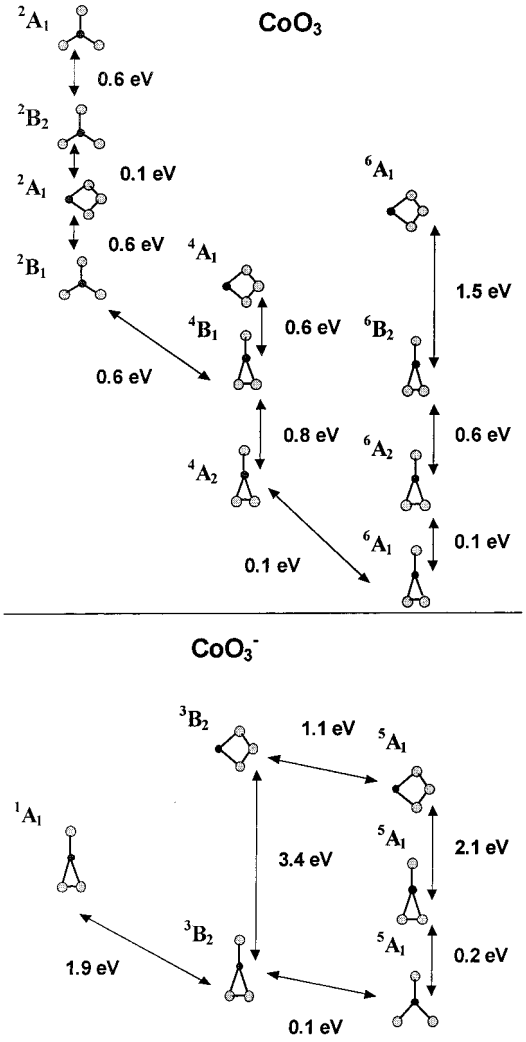

Figure 5. Local and global minima of CoO_3 and CoO_3^- clusters corresponding to oxoperoxides, oxides, and ozonides, ordered as to their relative energies and grouped according to spin multiplicity. The arrows (not to scale) denote the energy difference ΔE_{tot}, corresponding to adiabatic transitions.

it is comparable to that of the oxoperoxides, $OCoO_2$. Coupled-cluster calculations confirm the ordering of the states, as determined by B1LYP, but the energy differences between the states are calculated to be much lower, Table 11. Partial antiferromagnetic coupling was determined for the doublet state.

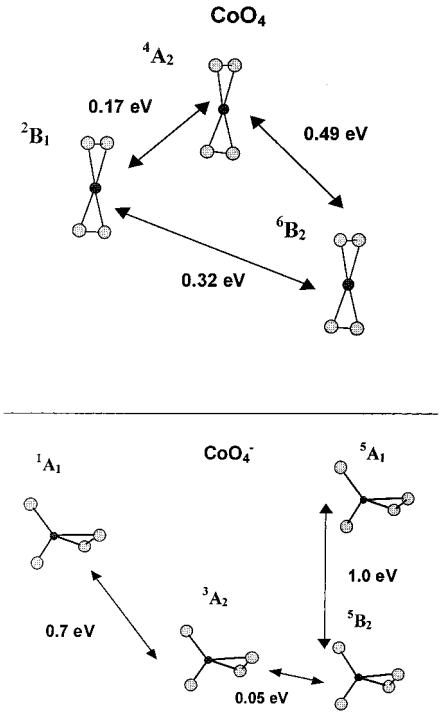

Figure 6. Local and global minima of CoO_4 and CoO_4^- clusters corresponding to oxoperoxides and diperoxides, ordered as to their relative energies and grouped according to spin multiplicity. The arrows (not to scale) denote the energy difference ΔE_{tot}, corresponding to adiabatic transitions.

The electron density on the oxygen atoms does not change with increasing spin multiplicity from quartet to sextet, Table 12.

Electron attachment to the diperoxides results in structural changes: breaking one O−O bond, elongating the CoO bonds, which form the peroxo fragment, and lowering the symmetry from D_{2d} to C_{2v}. For the lowest energy monoanion in the high-spin $^5B_2$ state, spin contamination was significant. The calculated adiabatic electron affinity is high, comparable to the affinity of dioxides, which form very stable monoanions; see Table 4. Antiferromagnetic coupling between Co and the peroxide oxygen atoms was found for the triplet and quintet states, Table 12.

Vibrational Modes. An intensive IR band in the 1000−1200 cm^{-1} range characterizes the diperoxides with D_{2d} symmetry, whereas for the monoanions, the most intensive IR band is at lower frequency; see Table 12. The irreducible representations

TABLE 11: Bond Lengths, Bond Angles and Energies for CoO_4 and CoO_4^-

CoO_4, D_2d Symmetry[a]							
cluster model	state	R_{Co-O}, Å	R_{O-O}, Å	∠OCoO, deg	$\langle S^2\rangle$	$\Delta E_{tot} \times 10^3$ Hartree B1LYP	$\Delta E_{tot} \times 10^3$ Hartree CCSD(T)
oxodiperoxide	$^6B_2$	1.926	1.336	40.6	8.777	0.00	(0.00)
	$^2B_1$	1.846	1.350	42.9	1.635	11.73	(1.22)
	$^4A_2$	1.951	1.320	39.5	4.672	18.05	(3.57)

CoO_4^-, C_2v Symmetry[b]								
cluster model	state	$R_{Co-O(1)}$,[c] Å	$R_{Co-O(2)}$,[c] Å	R_{O-O}, Å	$\angle O_{(1)}CoO_{(1)}$, deg	$\angle O_{(2)}CoO_{(2)}$, deg	$\langle S^2\rangle$	$\Delta E_{tot} \times 10^3$ Hartree B1LYP
oxoperoxide	$^5B_2$	1.772	2.082	1.335	114.5	37.4	7.033	0.00
	$^3A_2$	1.627	1.961	1.360	109.2	40.6	2.589	1.97
	$^1A_1$	1.612	1.798	1.420	114.7	46.5	0.000	29.23
	$^5A_1$	1.796	2.079	1.328	107.2	37.3	6.069	36.61

[a] ΔE_{tot} is the total energy difference relative to the ground state: $E_{tot} = -1683.41371$ Hartree for B1LYP, -1681.68386 Hartree for CCSD(T); CCSD(T) values given in parentheses. [b] ΔE_{tot} is the total energy difference relative to the ground state: $E_{tot} = -1683.52068$ Hartree. [c] Indexes (1) and (2) refer to oxygen atoms in the two perpendicular σ_v planes, respectively.

TABLE 12: Electronic Structure Parameters and Harmonic Vibrational Frequencies for CoO_4 and CoO_4^- [a]

CoO_4, D_{2d} symmetry			
	state		
	$^2B_1$	$^4A_2$	$^6B_2$
ω, cm^{-1}	90 e	83 e	183 b_1
	211 b_1	128 b_1	321 e (4)
	337 a_1	347 e	365 a_1
	338 e	379 a_1	477 b_2 (0)
	521 b_2	530 b_2	483 e (1)
	1099 b_2	1175 b_2	1144 a_1
	1108 a_1	1178 a_1	1153 b_2 (155)
ZPE, kJ mol^{-1}	24.71	25.43	29.49
DM, Debye	0.00	0.00	0.00
ESD_{Co}	2.07	0.38	2.44
ESD_O	−0.27	0.65	0.64
q_{Co}	0.52	0.52	0.55
q_O	−0.13	−0.13	−0.14

CoO_4^-, C_{2v} symmetry				
	state			
	$^1A_1$	$^3A_2$	$^5B_2$	$^5A_1$
ω, cm^{-1}	163 b_2	118 b_1 (40)	89 a_2	110 b_1
	198 b_1	163 a_2	109 b_1 (8)	119 a_2
	213 a_2	175 b_2 (10)	161 b_2 (14)	171 b_2
	324 a_1	214 b_2 (29)	168 a_1 (10)	175 a_1
	471 b_2	282 a_1 (0)	188 b_2 (15)	204 b_2
	561 a_1	307 a_1 (8)	273 b_1 (15)	369 a_1
	879 b_1	867 b_1 (167)	367 a_1 (57)	677 a_1
	911 a_1	875 a_1 (53)	655 a_1 (59)	1182 a_1
	991 a_1	1098 a_1 (69)	1179 a_1 (28)	1257 b_1
ZPE, kJ mol^{-1}	28.18	24.53	19.07	25.50
DM, Debye	0.98	1.53	2.20	2.42
ESD_{Co}	0.00	1.80	2.65	2.71
$ESD_{O(1)}$ [b]	0.00	0.45	1.12	1.07
$ESD_{O(2)}$ [b]	0.00	−0.34	−0.44	−0.42
q_{Co}	0.44	0.41	0.47	0.44
$q_{O(1)}$	−0.48	−0.48	−0.50	−0.51
$q_{O(2)}$	−0.24	−0.22	−0.24	−0.21

[a] Notations as in Table 2. IR intensities in km mol^{-1} for the low-energy states are given in parentheses. [b] Indexes 1 and 2 denote oxide and peroxide oxygen atoms, respectively.

for the symmetry modes of diperoxides with D_{2d} symmetry are $\Gamma = 2a_1(R) + b_1(R) + 2b_2(IR,R) + 2e(IR,R)$. The highest frequency IR-active mode is of b_2-symmetry and corresponds to the O−O stretching mode involving the two peroxo bonds in opposite phases. This is the highest intensity IR active vibration with a calculated isotopic ratio $^{16}O/^{18}O = 1.0599$ for the ground-state cluster. The in-phase O−O stretching mode is of a_1-symmetry and is expected at high-frequency according to the calculations.

The symmetry modes of the oxoperoxide monoanions span the irreducible representations $\Gamma = 4a_1(IR,R) + a_2(R) + 2b_1(IR,R) + 2b_2(IR,R)$. The a_2-modes are low-energy out-of-plane oxygen atom displacements. The a_1-stretching mode of the peroxo bond is the highest frequency one, 990−1200 cm^{-1}. The a_1-bending modes that involve the oxide oxygen atoms appear at 650−1100 cm^{-1}. The b_1-antisymmetric stretching mode of the oxide fragment is very sensitive to the cobalt−oxygen bond length and the angle OCoO. It appears at 273 cm^{-1} for the monoanion in its $^5B_2$ state. The same mode is found at 1257 cm^{-1} for the $^5A_1$ state monoanion.

Dissociation Paths

The CoO_n neutral species dissociate preferably with the release of molecular dioxygen. This is illustrated by the calculated dissociation energies; see Table 13. The calculated dissociation energy for CoO is in excellent agreement with the experimental value. [15] The CoO_n^- ($n = 1-3$) monoanions are thermodynamically more stable than the neutral parent molecules, due to the presence of low-lying unoccupied MOs in the neutral clusters. Ozonides are thermodynamically unstable and they lose molecular dioxygen in exothermal reactions. The release of atomic oxygen is less favorable and the heterolytic dissociation with ion formation is the least favorable. The energy

TABLE 13: Dissociation Schemes of CoO_n Species with Release of Oxygen[a]

	dissociation energy, eV	
reaction	D_0	$D_{(zpc)}$
Dissociation of Neutral Clusters		
$CoO \leftrightarrow Co + {}^1/_2O_2$	+1.34	+1.37
$CoO \leftrightarrow Co + O$	+3.83	+3.77 (+3.80)$_{exp}$ [15]
$CoO \leftrightarrow Co^+ + O^-$	+10.31	+10.25
$CoO_2 \leftrightarrow Co + O_2$	+2.11	+2.13
$CoO_2 \leftrightarrow CoO + O$	+3.18	+3.16
$CoO_2 \leftrightarrow Co^+ + O_2^-$	+9.56	+9.55
$CoO_2 \leftrightarrow Co^{2+} + O_2^{2-}$	+33.50	+33.49
$Co(O_2) \leftrightarrow Co + O_2$	+0.98	+0.96
$Co(O_2) \leftrightarrow CoO + O$	+2.06	+2.00
$Co(O_2) \leftrightarrow Co^+ + O_2^-$	+8.43	+8.39
$Co(O_2) \leftrightarrow Co^{2+} + O_2^{2-}$	+32.40	+32.33
$CoOO \leftrightarrow Co + O_2$	+0.98	+0.98
$CoOO \leftrightarrow Co^+ + O_2^-$	+8.43	+8.40
$OCo(O_2) \leftrightarrow CoO_2 + O$	+3.05	+2.96
$OCo(O_2) \leftrightarrow CoO + O_2$	+1.33	+1.32
$OCoOO \leftrightarrow CoO_2 + O$	+2.47	+2.38
$OCoOO \leftrightarrow CoO + O_2$	+0.75	+0.74
$Co(O_3) \leftrightarrow Co + O_3$	+3.47	+3.44
$Co(O_3) \leftrightarrow Co^{2+} + O_3^{2-}$	+31.21	+31.11
$Co(O_3) \leftrightarrow CoO + O_2$	−0.13	−0.19
$Co(O_3) \leftrightarrow CoO_2 + O$	+1.59	+1.45
$Co(O_2)_2 \leftrightarrow Co(O)_2 + O_2$	+1.43	+1.40
$Co(O_2)_2 \leftrightarrow OCo(O_2) + O$	+2.21	+2.08
$Co(O_2)_2 \leftrightarrow CoO_2 + O_2$	+0.36	+0.24
$Co(O_2)_2 \leftrightarrow CoO + {}^3/_2O_2$	+1.00	+0.99
$Co(O_2)_2 \leftrightarrow OCoOO + O$	+2.79	+2.66
$Co(O_2)_2 \leftrightarrow Co + 2O_2$	+2.44	+2.34
$Co(O_2)_2 \leftrightarrow CoOO + O_2$	+1.38	+1.39
Dissociation of Anion Clusters		
$CoO^- \leftrightarrow Co + {}^1/_2O_2^{2-}$	+6.19	+6.17
$CoO^- \leftrightarrow Co + O^-$	+3.88	+3.83
$CoO^- \leftrightarrow Co^+ + O^{2-}$	+19.26	+19.21
$CoO_2^- \leftrightarrow Co + O_2^-$	+4.84	+4.80
$CoO_2^- \leftrightarrow CoO^- + O$	+4.90	+4.83
$CoO_2^- \leftrightarrow CoO + O^-$	+4.95	+4.89
$CoO_2^- \leftrightarrow Co^+ + O_2^{2-}$	+19.88	+19.81
$Co(O_2)^- \leftrightarrow Co + O_2^-$	+2.30	+2.27
$Co(O_2)^- \leftrightarrow CoO^- + O$	+2.35	+2.30
$Co(O_2)^- \leftrightarrow CoO + O^-$	+2.41	+2.35
$Co(O_2)^- \leftrightarrow Co^+ + O_2^{2-}$	+17.34	+17.27
$CoO_3^- \leftrightarrow CoO^- + O_2$	+2.55	+2.54
$CoO_3^- \leftrightarrow CoO_2^- + O$	+2.56	+2.51
$CoO_3^- \leftrightarrow CoO + O_2^-$	+3.58	+3.54
$CoO_3^- \leftrightarrow CoO_2 + O^-$	+4.32	+4.24
$Co(O_3)^- \leftrightarrow CoO^- + O_2$	+0.22	+0.16
$Co(O_3)^- \leftrightarrow CoO_2^- + O$	+0.23	+0.13
$Co(O_3)^- \leftrightarrow CoO + O_2^-$	+1.24	+1.16
$Co(O_3)^- \leftrightarrow CoO_2 + O^-$	+1.99	+1.86
$CoO_4^- \leftrightarrow Co(O)_2 + O_2^-$	+3.99	+3.98
$CoO_4^- \leftrightarrow Co(O)_2^- + O_2$	+2.67	+2.68
$CoO_4^- \leftrightarrow OCo(O_2)^- + O$	+2.47	+2.44
$CoO_4^- \leftrightarrow CoO_2^- + O_2$	+0.13	+0.15
$CoO_4^- \leftrightarrow CoO_2 + O_2^-$	+2.86	+2.82
$CoO_4^- \leftrightarrow CoO^- + {}^3/_2O_2$	+2.93	+2.94
$CoO_4^- \leftrightarrow Co + O_2 + O_2^-$	+4.94	+4.92

[a] $Co(O_2)$, peroxide; CoOO, superoxide; $Co(O_3)$, ozonide; $Co(O_2)_2$, diperoxide. $D_{(zpc)}$, zero-point corrected dissociation energy.

required for dissociation to molecular oxygen is less than 1.5 eV, except from the ground state of the most stable quasilinear dioxide, CoO_2. The ground state of the linear CoO_2^- is thermodynamically the most stable one among all the structures studied. The thermodynamic stability of the neutral CoO_n species decreases in the order $CoO_2 > CoO > OCo(O_2) > Co(O_2) > OCoOO > Co(O_2)_2 > Co(O_3)$. For the monoanions the order of decreasing stability is in principle the same $CoO_2^- > CoO^- > CoO_3^- > Co(O_2)^- > CoO_4^- > Co(O_3)^-$. The overall stability of cobalt oxide species and their monoanions decreases in the order $CoO_2^- > CoO^- > CoO_3^- > Co(O_2)^- > CoO_2 > CoO > OCo(O_2) > Co(O_2) > OCoOO > Co(O_2)_2 > CoO_4^- > Co(O_3)^- > Co(O_3)$, showing that the anions take up the leading positions in this series. The dissociation paths of the cobalt dioxide anion and the cobalt peroxide anion with the release of an oxygen atom, dioxygen monoanion O_2^-, or oxygen monoanion O^- have comparable energies. Cobalt trioxide anions and cobalt ozonide anions dissociate with the loss of either atomic or molecular oxygen. The dissociation energies for the release of molecular dioxygen are only 0.03 eV higher than those for the release of atomic oxygen. Cobalt tetraoxide and the corresponding anion should dissociate preferably with the release of molecular oxygen. Due to the high stability of CoO_2^-, the dissociation of the monoanion CoO_4^- is less endothermic than that of the neutral cluster CoO_4.

The calculated dissociation energies of the studied CoO_n species are comparable with those for the copper oxide clusters[9] and are much lower than the dissociation energies for the iron oxide[8] and chromium oxide clusters.[10] Chromium oxide clusters are the most stable ones and their preferred dissociation path is the release of atomic oxygen.

Conclusions

The DFT study of CoO_n molecules and their anions reveals a variety of structures and a large number of closely spaced local minima on the potential energy surfaces, corresponding to low-lying excited or metastable states. The global minima are high-spin states—sextets for the neutral molecules and quintets for the anions, except for CoO, where the ground state is a quartet. The doublet state of linear CoO_2 corresponds to a saddle point with energy that is slightly higher than the energy of the bent molecule. Due to the small energy and structural differences between the two states, the linear arrangement may be fixed when CoO_2 is grafted in a solid-state matrix in case a favorable environment is provided. Oxide, oxoperoxide, oxosuperoxide, and ozonide chemical structures were found for CoO_3. The oxoperoxides are more stable than the oxides among the neutral species; the anionic species are thermodynamically more stable than the corresponding neutral parent molecules CoO_n ($n = 1-3$). Diperoxides are the stable configurations of the uncharged CoO_4 clusters. The most favorable dissociation path of the neutral species is the release of O_2. The dissociation of CoO_3^- and $Co(O_3)^-$ anions (trioxide and ozonide-like) may equally proceed with the release either of molecular dioxygen or of an oxygen atom. The quasilinear CoO_2 molecule in a $^6A_1$ state is thermodynamically the most stable neutral form and the linear CoO_2^- in a $^5\Delta$ state is the most stable anion.

Acknowledgment. We gratefully acknowledge CPU time at the Computer Center, Vienna University of Technology, where most of the Gaussian 98 calculations were performed.

References and Notes

(1) Simandi, L. I. *Dioxygen Activation and Homogeneous Catalytic Oxidation*; Elsevier: Amsterdam 1991.
(2) Ghanty, T. K.; Davidson, E. R. *J. Phys. Chem. A* **1999**, *103*, 8985.
(3) Ghanty, T. K.; Davidson, E. R. *J. Phys. Chem. A* **1999**, *103*, 2867.
(4) Archibong, E. F.; St-Amant, A. *J. Phys. Chem. A* **1998**, *102*, 6877.
(5) Pyykkö, P.; Tamm, T. *J. Phys. Chem. A* **1997**, *101*, 8107.
(6) Cao, Z.; Wu, W.; Zhang, Q. *J. Mol. Structure (THEOCHEM)* **1999**, *489*, 165.
(7) Gutsev, G. L.; Rao, B. K.; Jena, P. *J. Phys. Chem. A* **2000**, *104*, 11961.
(8) Gutsev, G. L.; Khanna, S. N.; Rao, B. K.; Jena, P. *J. Phys. Chem. A* **1999**, *103*, 5812.
(9) Nikolov, G. S.; Mikosch, H.; Bauer, G. *J. Mol. Structure (THEOCHEM)* **2000**, *499*, 35.
(10) Veliah, S.; Xiang, K.; Pandey, R.; Recio, J. M.; Newsam, J. M. *J. Phys. Chem. B* **1998**, *102*, 1126.
(11) Thomas, J. L. C.; Bauschlicher, C. W., Jr.; Hall, M. B. *J. Phys. Chem. A* **1997**, *101*, 8530.
(12) Deeth, R. J. *Structure and Bonding*; Springer-Verlag: Berlin, 1995; Vol. 82, p 1.
(13) Siegbahn, P. E. M. In *Advances in Chemistry and Physics*; Prigogine, I., Rice, S., Eds.; John Wiley & Sons Inc.: New York, 1996; Vol. XCIII, p 333.
(14) Gutsev, G. L.; Rao, B. K.; Jena, P. *J. Phys. Chem. A* **2000**, *104*, 5374.
(15) Huber, K. P.; Herzberg, G. *Constants of Diatomic Molecules*; van Nostrand Reinhold: New York, 1979.
(16) Adam, A. G.; Azuma, Y.; Barry, J. A.; Huang, G.; Lyne, M. P.; Merer, A.; Schröder, J. O. *J. Chem. Phys*. **1987**, *86*, 5231.
(17) Chertihin, G. V.; Citra, A.; Andrews, L.; Bauschlicher, C. W., Jr. *J. Phys. Chem*. *A* **1997**, *101*, 8793.
(18) Van Zee, R. J.; Hamrick, Y. M.; Li, S.; Weltner, W., Jr. *J. Phys. Chem*. **1992**, *96*, 7247.
(19) Frisch, M. J.; Trucks, G. W.; Schlegel, H. B.; Scuseria, G. E.; Robb, M. A.; Cheeseman, J. R.; Zakrzewski, V. G.; Montgomery, J. A., Jr.; Stratmann, R. E.; Burant, J. C.; Dapprich, S.; Millam, J. M.; Daniels, A. D.; Kudin, K. N.; Strain, M. C.; Farkas, O.; Tomasi, J.; Barone, V.; Cossi, M.; Cammi, R.; Mennucci, B.; Pomelli, C.; Adamo, C.; Clifford, S.; Ochterski, J.; Petersson, G. A.; Ayala, P. Y.; Cui, Q.; Morokuma, K.; Malick, D. K.; Rabuck, A. D.; Raghavachari, K.; Foresman, J. B.; Cioslowski, J.; Ortiz, J. V.; Stefanov, B. B.; Liu, G.; Liashenko, A.; Piskorz, P.; Komaromi, I.; Gomperts, R.; Martin, R. L.; Fox, D. J.; Keith, T.; Al-Laham, M. A.; Peng, C. Y.; Nanayakkara, A.; Gonzalez, C.; Challacombe, M.; Gill, P. M. W.; Johnson, B.; Chen, W.; Wong, M. W.; Andres, J. L.; Head-Gordon, M.; Replogle, E. S.; and Pople, J. A. *Gaussian 98*, Revision A.3; Gaussian, Inc.: Pittsburgh, PA, 1998.
(20) Becke, A. D. *J. Chem. Phys.* **1996**, *104*, 1040.
(21) Lee, C.; Yang W.; Parr, R. G. *Phys. Rev.* **1988**, *B37*, 785−789.
(22) Miehlich, B.; Savin, A.; Stoll, H.; Preuss, H. *Chem. Phys. Lett.* **1989**, *157*, 200.
(23) Becke, A. D. *J. Chem. Phys.* **1993**, *98*, 5648.
(24) Pople, J. A.; Krishnan, R.; Schlegel, H. B.; Binkley, J. S. *Int. J. Quantum Chem.* **1978**, *XIV*, 545.
(25) Cizek, J. *Adv. Chem. Phys.* **1969**, *14*, 35.
(26) Purvis, G. D.; Bartlett, R. J. *J. Chem. Phys.* **1982**, *76*, 1910.
(27) Scuseria, G. E.; Janssen, C. L.; Schaefer, H. F., III. *J. Chem. Phys.* **1988**, *89*, 7382.
(28) Scuseria, G. E.; Schaefer, H. F., III. *J. Chem. Phys.* **1989**, *90*, 3700.
(29) Pople, J. A.; Head-Gordon, M.; Raghavachari, K. *J. Chem. Phys.* **1987**, *87*, 5968.
(30) Mulliken, R. S. *J. Chem. Phys.* **1955**, *23*, 1833.
(31) Almlöf, J.; Taylor, P. R. *J. Chem. Phys.* **1987**, *86*, 4070.
(32) Glendening, E. D.; Reed, A. E.; Carpenter, J. E.; Weinhold, F. NBO Version 3.1.
(33) Reed, A. E.; Curtiss L. A.; Weinhold, F. *Chem. Rev.* **1988**, *88*, 899.
(34) Cotton, F. A.; Wilkinson, G. *Advanced Inorganic Chemistry*, 3rd ed.; Wiley-Interscience: New York, 1988.
(35) Wells, A. *Structural Inorganic Chemistry*; Clarendon Press: Oxford, U.K., 1986.
(36) (a) Nakamoto, K. *Infrared and Raman Spectra of Inorganic and Coordination Compounds*; Wiley-Interscience: New York, 1978. (b) Barbe, A.; Secroun, C.; Jouve, P. *J. Mol. Spectrosc.* **1974**, *49*, 171.
(37) Gelotta, R. H.; Bennet, R. A.; Hall, J. L.; Siegel, M. W.; Levine, J. *Phys. Rev. A* **1972**, *6*, 631.
(38) Bauschlicher, C. W., Jr.; Maitre, P. *Theor. Chim. Acta* **1995**, *90*, 189.
(39) Li, X.; Wang, L. S. *J. Chem. Phys*. **1999**, *111*, 8389.
(40) Burdett, J. K. *Molecular Shapes*; J. Wiley & Sons: New York, 1980; p 68.
(41) Albright, T.; Burdett, J.; Whangbo, M.-H. *Orbital Interactions in Chemistry*; J. Wiley & Sons: New York, 1985.